Study on the Mechanism of the Effect of Temperature on the Decomposition Reaction of SFn (n=1-6) under Discharge Conditions

Minghao Yang (ymh3119304251@stu.xjtu.edu.cn)
Xi'an Jiaotong University https://orcid.org/0000-0003-1758-4658
Jing Yan
Xi'an Jiaotong University
Mengyuan Xu
Xi'an Jiaotong University
Yingsan Geng
Xi'an Jiaotong University
Zhiyuan Liu
Xi'an Jiaotong University
Jianhua Wang
Xi'an Jiaotong University

Research Article

Keywords: gibbs free energy change, electronic impact, quantum chemistry, reaction mechanism

Posted Date: April 19th, 2021

DOI: https://doi.org/10.21203/rs.3.rs-388556/v1

Version of Record: A version of this preprint was published at Journal of Molecular Modeling on August 5th, 2021. See the published version at https://doi.org/10.1007/s00894-021-04866-2.

Study on the Mechanism of the Effect of Temperature on the Decomposition Reaction of SF_n (n=1-6) under Discharge Conditions

Minghao Yang, Jing Yan*, Mengyuan Xu, Yingsan Geng, Zhiyuan Liu and Jianhua Wang
Author to whom correspondence should be addressed: yanjing@mail.xjtu.edu.cn
State Key Laboratory of Electrical Insulation and Power Equipment
Xi'an Jiaotong University
Xi'an, P. R. China

ABSTRACT

The study on the mechanism of the effect of temperature on the decomposition reaction of SF_n (n=1-6) under discharge conditions is very important in studying the potential fault of SF_6 high voltage switch equipment and perfecting the chemical kinetic model of SF_n discharge. In this paper, structural optimizations, vibrational frequency calculations, and zero-point energy calculations for the reactants and products were performed at the B3LYP/6-311++G(d,p) theory level. The single-point energies of all species were collected at the CCSD(T)/aug-cc-PVTZ level. The electric and thermal decomposition mechanism of SF_n under discharge conditions of 298K–10000K were studied, respectively. The conclusion drawn was that in the temperature range of 298–10000K, the thermal decomposition homopolytic reaction △G began to decline from 200 kJ/mol, while the △G of the other two heterogenous reactions began to decrease from 1000 kJ/mol and 2000 kJ/mol, showing a downward trend of an almost similar slope. The electrolysis of SF_n is related to the electron energy. When the electron energy is low, $SF_n + e \rightarrow SF_n^-$ series reactions occur, and △G of R12, R20, R28, R36, R44 increases with temperature rise, while △G of R4 decreases with temperature. When the electron energy is high, one of $SF_n^- \rightarrow SF_{n-1}^- + F$、$SF_n^- \rightarrow SF_{n-1} + F^-$ and $SF_n^- \rightarrow SF_{n-1} + F + e$ will occur, and the reactions that occur at various temperature ranges as the temperature rises vary. When the second electron hits the SF_n^-, the $SF_n^- + e \rightarrow SF_{n-1}^- + F$ reaction will occur. The △G of this reaction slowly decreases with an increase in temperature. This study in clearer terms explains the decomposition process and mechanism of SF_n at different temperatures.

Keywords: gibbs free energy change, electronic impact, quantum chemistry, reaction mechanism

INTRODUCTION

SF_6 high voltage switch equipment has a number of advantages. These include small size, high safety, and long maintenance period. With the improvement of power system voltage level, SF_6 high voltage switch equipment use has drastically grown. SF_6 is a colorless, tasteless, non-toxic, non-flammable stable gas. Because of its good electron affinity, thermodynamic stability and good dielectric property , it is commonly used as insulating medium and arc extinguishing medium for gas insulated equipment [1]. However, when partial discharge or arc discharge occurs in the equipment, SF_6 gas will decompose on reacting with heat and electricity and form neutral low-flourine flourosulfur species, such as SF_5, SF_4, SF_3, SF_2, SF, and anions SF_6^-, SF_5^-, SF_4^-, SF_3^-, etc. [2-4]. Most of the low-fluorine sulfides (99.9%) will react with F atoms to regenerate SF_6 in a very short period of time. But a small part will

react with trace amount of water and oxygen inside the equipment in a series of complex chemical reactions, and finally produce SOF_4, SOF_2, SO_2F_2, HF, SO_2, CF_4, CO_2, CS_2 and other by-products[5]. As much as these products reduce the purity of SF_6 gas and affect its insulation and arc extinguishing performance, they also corrode the metal parts and solid insulating materials in the equipment, lowering the durability of the equipment. On the other hand, the components and contents of some characteristic products can be utilized in evaluating the deterioration of the metal and solid insulating materials in the equipment, and to identify the discharge defects in the equipment.

Many scholars have done a lot of research on the decomposition products of SF_6 under discharge conditions. Local overheating is an important cause of decomposition of SF_6 molecule. Wilkins found through experimental research that at a temperature 1500K, the main decomposition product of SF_6 gas is SF_4 [6]. W·Frie used the counter ion concentration calculation method to roughly estimate the number of equilibrium particles in SF_6 plasma at various temperatures [7]. It was found that when the temperature of SF_6 gas was higher than 1500K, its concentration was significantly minimal, and the SF_4 concentration and F atoms would rise rapidly. At temperatures higher than 4000K, most of the SF_6 molecules would be completely decomposed, but the decomposition mechanism has not been further studied. Under arc discharge, electron collision is another key factor affecting the decomposition of SF_6 molecules. As early as 1953, AJ Ahearn et al. discovered that the main products of SF_6 molecules ionized by electron impact in vacuum are SF_6^-, SF_5^- and F^- plasma [8]. Wiggart N and Wang Y et al. believed that SF_6 was a strongly electronegative gas, which if combined with electrons would form metastable molecular group $(SF_6)^*$. After a very short time, the molecular group will further generate SF_6^-, SF_5^-, F^- and other anions. On further increase to the electron energy, SF_4^-, SF_3^- and other anion low-fluoride sulfide may be formed [9, 10]. Zieglar et al. theoretically studied the decomposition process of anion low-fluoride sulfide, and found that further decomposition of SF_5^-, SF_4^-, SF_3^-, SF_2^-, SF^- and other anions would lead to a formation of a lower level of neutral low-fluoride sulfide molecule and an F^- anion, but he did not take a keen note on the process in which electrons participate in the reaction [2]. Fifen found that the thermodynamic data of electrons would vary greatly with temperature change, and he corrected the thermodynamic data of 0–10000K through algorithm iteration [11]. Wang et al. studied the particle compositions of an SF_6 arc using a two-temperature chemical kinetics model. The chemical reaction system consists of 18 particles, and 63 chemical reactions are taken into consideration. But they did not consider the effect of temperature change on the reaction, and did not include reactions involving SF_2^- andSF_3^-. The chemical reaction equation was incomplete [12].

Early research mainly focused on the qualitative analysis of the types of SF_6 gas decomposition products. The thermal decomposition mechanism and electron impact decomposition mechanism of SF_n at different temperatures has not been systematically studied. This paper systematically combs the decomposition process of SF_n, discharge decomposition products in different temperature ranges, and gives a detailed explanation of the decomposition process of SF_n at different temperatures. In addition, it has certain guiding significance for a further study on the reaction of SF_6 with micro water and micro oxygen at different temperatures. This paper

uses quantum chemistry theory to systematically comb the decomposition products and processes of SF_n at a temperature of 298–10000K. The second part describes the calculation method, and the third part provides the results and discussion. In addition, this article also has certain reference significance for establishing a complete arc plasma model.

2 CALCULATION METHOD

In this paper, quantum chemistry method is used to find out the reaction mechanism of SF_n (n = 1-6) under overheating and electron impact conditions under discharge conditions. Table 1 lists all the reaction equations in this paper. It is divided into two types of processes: overheating decomposition and electron impact decomposition. Taking the decomposition of SF_6 as an example, R1 is the process of covalent bond homolysis resulting from overheating, R2 and R3 are the process of covalent bond heterolysis, R4 and R8 are electron capture process while R5, R6, and R7 are decomposition processes resulting from R4.

Table 1. All reaction equations in this paper

Serial number	Chemical reaction
R1	$SF_6 \rightarrow SF_5 + F$
R2	$SF_6 \rightarrow SF_5^+ + F^-$
R3	$SF_6 \rightarrow SF_5^- + F^+$
R4	$SF_6 + e \rightarrow SF_6^-$
R5	$SF_6^- \rightarrow SF_5^- + F$
R6	$SF_6^- \rightarrow SF_5 + F^-$
R7	$SF_6^- \rightarrow SF_5 + F + e$
R8	$SF_6^- + e \rightarrow SF_5^- + F^-$
R9	$SF_5 \rightarrow SF_4 + F$
R10	$SF_5 \rightarrow SF_4^+ + F^-$
R11	$SF_5 \rightarrow SF_4^- + F^+$
R12	$SF_5 + e \rightarrow SF_5^-$
R13	$SF_5^- \rightarrow SF_4^- + F$
R14	$SF_5^- \rightarrow SF_4 + F^-$
R15	$SF_5^- \rightarrow SF_4 + F + e$
R16	$SF_5^- + e \rightarrow SF_4^- + F^-$
R17	$SF_4 \rightarrow SF_3 + F$
R18	$SF_4 \rightarrow SF_3^+ + F^-$
R19	$SF_4 \rightarrow SF_3^- + F^+$
R20	$SF_4 + e \rightarrow SF_4^-$
R21	$SF_4^- \rightarrow SF_3^- + F$
R22	$SF_4^- \rightarrow SF_3 + F^-$
R23	$SF_4^- \rightarrow SF_3 + F + e$
R24	$SF_4^- + e \rightarrow SF_3^- + F^-$
R25	$SF_3 \rightarrow SF_2 + F$
R26	$SF_3 \rightarrow SF_2^+ + F^-$
R27	$SF_3 \rightarrow SF_2^- + F^+$
R28	$SF_3 + e \rightarrow SF3^-$
R29	$SF_3^- \rightarrow SF_2^- + F$
R30	$SF_3^- \rightarrow SF_2 + F^-$
R31	$SF_3^- \rightarrow SF_2 + F + e$
R32	$SF_3^- + e \rightarrow SF_2^- + F^-$
R33	$SF_2 \rightarrow SF + F$
R34	$SF_2 \rightarrow SF^+ + F^-$
R35	$SF_2 \rightarrow SF^- + F^+$
R36	$SF_2 + e \rightarrow SF_2^-$
R37	$SF_2^- \rightarrow SF^- + F$
R38	$SF_2^- \rightarrow SF + F^-$
R39	$SF_2^- \rightarrow SF + F + e$
R40	$SF_2^- + e \rightarrow SF^- + F^-$
R41	$SF \rightarrow S + F$
R42	$SF \rightarrow S^+ + F^-$
R43	$SF \rightarrow S^- + F^+$
R44	$SF + e \rightarrow SF^-$
R45	$SF^- \rightarrow S- + F$
R46	$SF^- \rightarrow S + F^-$
R47	$SF^- \rightarrow S + F + e$
R48	$SF^- + e \rightarrow S^- + F^-$

Table 2. Entropy, enthalpy and Gibbs free energy of gaseous electrons

T (K)	S (J/mol)	H (kJ/mol)	G (kJ/mol)
298.15	22.6432	3.1351	-3.616
300	22.7491	3.1659	-3.6588
350	25.4629	4.0467	-4.8653
400	27.9153	4.9654	-6.2008
450	30.1427	5.9111	-7.6531

500	32.1769	6.8766	-9.2118
600	35.7696	8.8478	-12.6139
700	38.8607	0.8534	-16.3491
800	41.5666	12.88	-20.3733
900	43.9694	14.9201	-24.6523
1000	46.1284	16.9694	-29.159
2000	60.4503	37.6429	-83.258
3000	68.8664	58.4007	-148.199
4000	74.8428	79.1749	-220.196
5000	79.4797	99.9548	-297.443
6000	83.2687	120.7372	-378.875
7000	86.4725	141.5209	-463.787
8000	89.2479	162.3053	-551.678
9000	91.696	183.0902	-642.174
10000	93.886	203.8754	-734.984

All the calculations of quantum chemistry in this study are completed in Gaussian 09 [17]. Gausian 09 is currently the most popular and powerful quantum chemical calculation software. So as to predict the accuracy of the outcome, the article uses M06-2X/def2-TZVP level and B3LYP/6-31G(d) level and B3LYP/6-311++G(d, P) level for verification and comparison. The above levels were used to optimize the structure of reactants and products, and calculate the vibration frequency and zero-point energy [13]. Thermodynamic data consists of the sum of single point energy and thermal correction. Because the calculation of the thermal correction does not require a high level of calculation to get a very accurate result. The thermal correction was obtained at the B3LY P/6-311++G(d, p) level. Single point energy requires a high level of calculation to get accurate results, so single-point energy calculation was done at the CCSD(T)/aug-cc-PVTZ level [14]. To ensure accuracy in the calculated outcome, the frequency vibration factor is considered. When using the B3LYP/6-311++G(d, p) level, the frequency vibration factor is 0.967. Because of some limitations of Gaussian 09 in obtaining thermodynamic data, this paper used the KisTheIP to obtain thermodynamic data of all structures at 298–10000K [15]. KisTheIP is a program renown for calculating chemical reaction rates and thermodynamic data. It has many functions which include calculating thermodynamic data, calculating reaction equilibrium constants, calculating the reaction rate constants of single or bimolecular reactions by TST or VTST methods, and some more. For the record, KisTheIP cannot get the thermodynamic data of electrons. The thermodynamic data of electrons used in this paper uses the thermodynamic data mentioned in the Fifen's article as shown in Table 2, and is derived to by fitting the cubic spline difference [11]. The Gibbs free energy of gas phase electrons changes with temperature as shown in Figure 1. After obtaining the thermodynamic data of all the structures, △G of all the reactions in this paper was got by subtracting G of the reactants from G of the products. For example, at 298K, for the reaction $SF_6 \rightarrow SF_5 + F$ in Table 3, the G of the reactant SF_6 is -996.1496484Hartree, the G of the product SF_5 is -896.3641003Hartree, the G of F is -99.64262951Hartree, the △G of this reaction is:

$$\Delta G = \left(-896.3641 - 99.6426295 + 996.1496484\right) \times 2625.5 = 375.2\text{kJ / mol}$$

Calculate the △G of all reactions in the temperature range of 298-10000K, and get the curve in Figure 3-10.

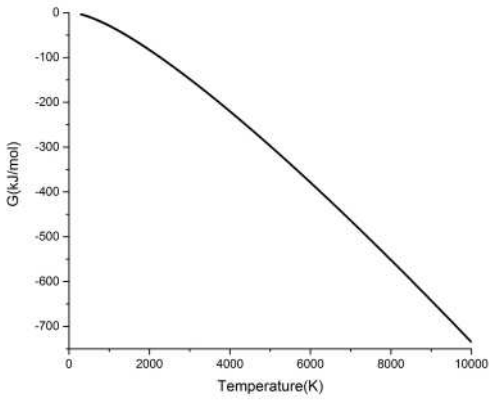

Figure 1. Gibbs free energy of gas phase electrons changes with temperature

3 RESULTS AND DISCUSSION

3.1 STRUCTURAL OPTIMIZATIONS AND ENERGIES

The optimized structure of reactants and products in reaction R1-R48 is displayed in Figure 2. In this paper, structural optimization was performed at the B3LYP/6-311++G(d,p) level of theory. The optimized structure of all neutral reactants and products was compared with the experimental geometric data in the NIST database and the outcomes of other theoretical calculations (B3LYP/6-31g (d)) [18]. The structural parameters of all reactants and products coincide with the literature of Tom Ziegler and Cheung [2,16]. The key structural parameters are shown in Figures 2. The B3LYP/6-311++G(d, p) level not only provides excellent computing accuracy, but also significantly saves computing resources. In comparison to the experimental data, the bond Angle error of all structures was <0.1Å, and the bond length error of all structures was <2.6°. The error mainly results from the difference of theoretical level.

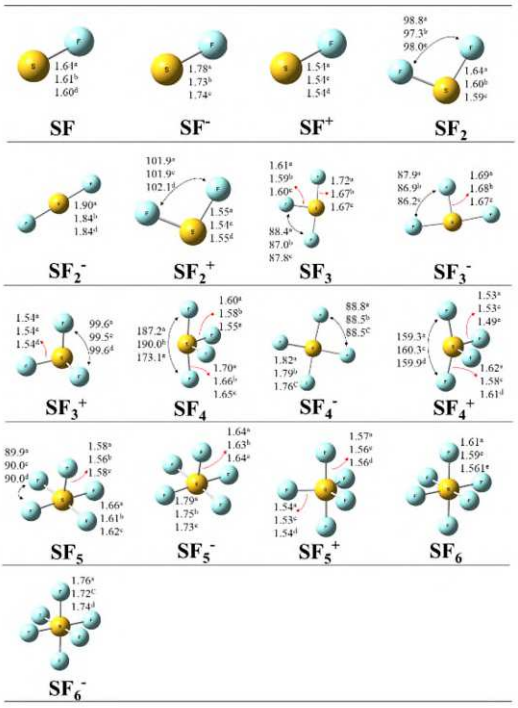

Figure 2. Optimized structures of all reactants and products. (Bond lengths are in angstroms and bond angles are in degrees.)

a. B3LYP/6-311++G(d, p) level in the present work.

b. Equilibrium structures in the Tom Ziegler's work.

c. Equilibrium structures in the Cheung's work.

d. B3LYP/6-31G(d) level in the NIST database.

e. Experimental geometry data in the NIST database.

Table 3. △G of reactions at 298, 5000, and 10000K temperatures

Chemical reaction	**298K**	**5000K**	**10000K**
$SF_6 \rightarrow SF_5 + F$	375.2	−434.3	−1274.0
$SF_6 \rightarrow SF_5^+ + F^-$	1004.3	334.5	−353.0
$SF_6 \rightarrow SF_5^- + F^+$	1913.5	1010.7	70.0
$SF_6 + e \rightarrow SF_6^-$	−126.1	−246.5	−255.5
$SF_6^- \rightarrow SF_5^- + F$	105.2	−410.4	−933.3
$SF_6^- \rightarrow SF_5 + F^-$	187.1	−181.1	−545.4
$SF_6^- \rightarrow SF_5 + F + e$	501.3	−187.8	−1018.5
$SF_6^- + e \rightarrow SF_5^- + F^-$	−209.0	−403.6	−460.3

$SF_5 \rightarrow SF_4 + F$	−53.4	−867.5	−1712.1
$SF_5 \rightarrow SF_4^+ + F^-$	936.2	309.1	−333.3
$SF_5 \rightarrow SF_4^- + F^+$	1884.6	1097.6	281.8
$SF_5 + e \rightarrow SF_5^-$	−396.1	−222.5	85.2
$SF_5^- \rightarrow SF_4^- + F$	346.4	−347.5	−1062.2
$SF_5^- \rightarrow SF_4 + F^-$	215.9	−267.7	−756.0
$SF_5^- \rightarrow SF_4 + F + e$	530.1	−274.4	−1229.1
$SF_5^- + e \rightarrow SF_4^- + F^-$	32.2	−340.7	−589.2
$SF_4 \rightarrow SF_3 + F$	372.6	−300.6	−993.6
$SF_4 \rightarrow SF_3^+ + F^-$	1120.3	590.6	52.6
$SF_4 \rightarrow SF_3^- + F^+$	1954.0	1303.4	633.4
$SF_4 + e \rightarrow SF_4^-$	−183.7	−73.0	166.8
$SF_4^- \rightarrow SF_3^- + F$	203.3	−291.2	−792.3
$SF_4^- \rightarrow SF_3 + F^-$	242.1	−220.8	−687.4
$SF_4^- \rightarrow SF_3 + F + e$	556.3	−227.6	−1160.4
$SF_4^- + e \rightarrow SF_3^- + F^-$	−110.9	−284.4	−319.3
$SF_3 \rightarrow SF_2 + F$	144.5	−371.7	−896.4
$SF_3 \rightarrow SF_2^+ + F^-$	819.6	329.8	−165.8
$SF_3 \rightarrow SF_2^- + F^+$	2007.5	1568.5	1149.4
$SF_3 + e \rightarrow SF3^-$	−353.0	−63.6	368.1
$SF_3^- \rightarrow SF_2^- + F$	426.1	−35.5	−477.6
$SF_3^- \rightarrow SF_2 + F^-$	183.3	−301.4	−791.4
$SF_3^- \rightarrow SF_2 + F + e$	497.5	−308.1	−1264.5
$SF_3^- + e \rightarrow SF_2^- + F^-$	111.9	−28.8	−4.5
$SF_2 \rightarrow SF + F$	303.5	−223.3	−784.7
$SF_2 \rightarrow SF^+ + F^-$	1117.2	657.3	167.5
$SF_2 \rightarrow SF^- + F^+$	2033.3	1544.5	1023.0
$SF_2 + e \rightarrow SF_2^-$	−71.4	272.6	786.9
$SF_2^- \rightarrow SF^- + F$	170.3	−395.7	−1022.8
$SF_2^- \rightarrow SF + F^-$	60.7	−489.1	−1098.5
$SF_2^- \rightarrow SF + F + e$	374.9	−495.9	−1571.6
$SF_2^- + e \rightarrow SF^- + F^-$	64.3	−191.6	−363.6
$SF \rightarrow S + F$	302.9	−173.1	−705.6
$SF \rightarrow S^+ + F^-$	1172.5	739.5	252.7
$SF \rightarrow S^- + F^+$	2053.8	1620.8	1134.0
$SF + e \rightarrow SF^-$	−204.6	100.2	548.8
$SF^- \rightarrow S- + F$	324.1	−147.0	−673.7
$SF^- \rightarrow S + F^-$	193.2	−266.6	−781.3
$SF^- \rightarrow S + F + e$	507.4	−273.3	−1254.4
$SF^- + e \rightarrow S^- + F^-$	9.9	−140.2	−200.6

Table 3 shows the △G of all reactions at 298K, 5000K, and 10000K. From the data in Table 3, we can roughly see the trend of the △G of reactions with the change of temperature, which is more clearly compared with Figure 3-10. The △G is in kJ/mol in Table 3.

3.2 REACTION MECHANISMS

During the installation and operation of SF_6 high voltage switchgear, electrode surface burrs, free conducting particles and suspension potential may exist in the equipment, leading to partial discharge or overheating in the equipment, making the gas temperature near the fault center higher compared to the ambient temperature. Under the parameters of arc and spark discharge, the decomposition of SF_6 mostly results from electron impact or high temperature. Under partial discharge and corona discharge, SF_6 dissociation is as a result of electron collisions in the discharge area due to low temperature. In this paper, the influence of different temperature on SF_n decomposition reaction is considered, and Gibbs free energy is utilized in the analysis of each reaction.

3.2.1 Thermal decomposition of SF_n (n = 1~6) under overheating conditions

The SF_6 discharge decomposition reaction equation of SF_6 high voltage switchgear is shown in Table 1. As Table 1 displays, the decomposition of SF_6 is the process of S-F bond breaking in its molecular structure to form free radicals. The thermal decomposition process of SF_6 may be directly decomposed into SF_5 and F atoms, or heterocracking of covalent bonds may lead to formation of SF_5^+, F^-, or SF_5^-, F^+. Figure 3 shows the change of △G of R1, R2, and R3 at the temperature of 298–10000K. Figure 3 shows that the △G of R1-R3 decreases linearly with the increase of temperature. The △G of R1 at 298K is 375.2kJ/mol. When the

temperature reaches about 2450K, △G falls below 0kJ/mol, and the reaction can proceed spontaneously. When the temperature reaches 10000K, △G drops to −1274kJ/mol. The △G of R2 at 298K is 1004.3kJ/mol, when the temperature reaches about 7400K, the △G of reaction can drop below 0kJ/mol, when the temperature reaches 10000K, the △G of reaction is −353kJ/mol. The △G of R3 at 298K is 1913.5kJ/mol, when the temperature reaches 10000K, △G is 70kJ/mol, and it does not drop below 0kJ/mol. Therefore, for the thermal decomposition process of SF_6, R1 is most likely to occur within the temperature range of 298–10000K.

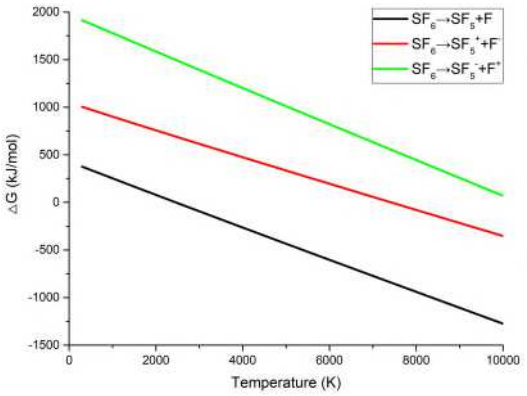

Figure 3. SF_6 thermal decomposition △G changes with temperature

The thermal decomposition process of SF_5 may directly decompose SF_4 and F atoms, or the covalent bond may heterocrack to produce SF_4^+, F^-, or SF_4^-, F^+. The SF_5 thermal decomposition △G changes with temperature as Figure 4 shows. It can be seen from Figure 4 that △G of R9-R11 also decreases linearly with the temperature rise. During the thermal decomposition of SF_5, the △G of R9 at 298K is −53.4kJ/mol, when the temperature reaches 10000K, the △G decreases to −1712.1kJ/mol. The △G of R10 at 298K is 936.2kJ/mol, when the temperature reaches about 7400K, △G drops below 0kJ/mol, and the reaction can be spontaneous. When the temperature reaches 10000K, △G drops to −333.3kJ/mol. The △G of R11 at 298K is 1884.6kJ/mol, when the temperature reaches 10000K, △G decreases to 281.8kJ/mol. Therefore, for the thermal decomposition process of SF_5, R9 will most probably occur within the temperature range of 298–10000K.

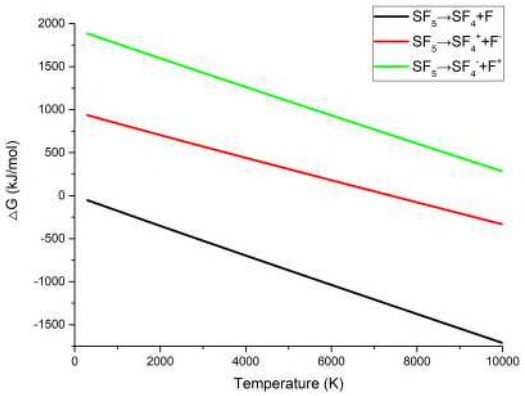

Figure 4. SF_5 thermal decomposition △G changes with temperature

From the above analysis, it can be seen that △G of SF_n displayed similar thermal decomposition rules within the temperature range of 298–10000K, and there was a decrease in energy required for the reaction as the temperature increased. Moreover, the energy required for the homolytic reaction is far less than the other two heterolytic reactions, so the homolytic reaction is most probable to take place. This is because SF_n and F are both highly electronegative molecules. It is very hard for each molecule to lose electron and need to absorb a lot of energy. In addition, the same is the heterolytic dissociation, the reactions R2 and R10 can proceed spontaneously as the temperature increases, but the reactions R3 and R11 still cannot proceed spontaneously at very high temperatures. This is because the electronegativity of F is greater than that of SF_n (n=1-5), so the stability of SF_n^+ in the product is better than F^+ [19]. The reaction process curve and mechanism of other reactants SF_m (m=1-4) are similar to that of SF_5 and SF_6. Please refer to the supplementary materials for details.

3.2.2 The electron impact decomposition process of SF_n (n = 1-6)

SF_n in gas insulation equipment will be decomposed by energy because of electron impact in addition to simple thermal decomposition. Figure 5 shows the change of △G of R4-R8 reaction at 298–10000K. From Figure 5 we realize that △G of R4-R8 showed a decreasing trend with the increase of temperature. SF_6 is a highly electronegative gas. When the energy of electrons in space is low, SF_6 can be combined with electrons in space to form a metastable molecular group $(SF_6)^*$. In a short while, this molecular group can further generate anion SF_6^-. That is, R4: $SF_6 + e \rightarrow SF_6^-$. When the temperature is 298K, △G is 126.1kJ/mol, when the temperature rises to 5000K, △G is −246.5kJ/mol, when the temperature reaches 10000K, △G is −255.5kJ/mol. With the temperature rise, the △G of this reaction was less than zero, so it could proceed spontaneously.

When electrons continue to hit SF_6^-, R8: $SF_6^- + e \rightarrow SF_5^- + F$- occurs. When the temperature is 298K, △G is 209kJ/mol, when the temperature rises to 5000K, △G is −403.6kJ/mol, when the temperature reaches 10000K, △G is −460.3kJ/mol. The △G of this reaction is also less than zero, and goes on spontaneously.

When the energy of electrons hitting SF_6 is high, $SF_6 + e \rightarrow SF_6$- reaction will occur first, and then SF_6^- will be decomposed because of the huge energy of electrons, and three reactions of R5-R7 may occur: $SF_6^- \rightarrow SF_5^- + F$, $SF_6^- \rightarrow SF_5 + F^-$, $SF_6^- \rightarrow SF_5 + F + e$. At a temperature 298K, the △G of R5 is 105.2 kJ/mol, with a rise to about 1200K, it decreases to 0 kJ/mol, when the temperature reaches 10000K, the △G is −933.3 kJ/mol. The △G of R6 at 298K is 105.2 kJ/mol, when the temperature increases to about 2600K, it drops to 0 kJ/mol, when the temperature reaches 10000K, △G is −545.4 kJ/mol. The △G of R7 at 298K is 501.3kJ/mol, when the temperature rises to about 3800K, it drops to 0 kJ/mol, and when the temperature reaches 10000K, the △G is −1018.5 kJ/mol. Since the curve of reaction R5-7 has an intersection point in the temperature range of 298–10000K, the reaction that takes place with temperature rise varies. At 298–8700K, R5 has the lowest △G, so it is most likely to occur. The reaction produces SF_5^- and F. The △G of R7 is the lowest at 8700–10000K, and the probability of R7 is greater in this temperature range.

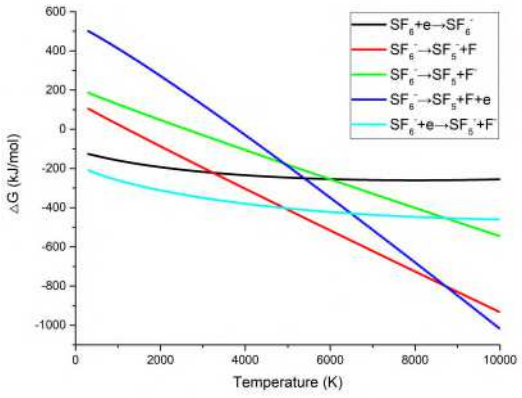

Figure 5. SF_6 electron impact decomposition process △G changes with temperature

Figure 6 shows the change of ΔG of the R12-R16 reaction at a temperature of 298–10000K. It can be seen from Figure 6 that the △G of R13-R16 shows a downward trend with temperature rise, but the △G of R12 increases with increasing temperature. When the electron energy in the space is low, the R12 reaction will occur: $SF_5 + e \rightarrow SF_5^-$. When the temperature is 298K, the △G is −396.1 kJ/mol, when the temperature is increased to 5000K, the △G is −222.5kJ/mol, when the temperature reaches 10000K, the △G is 85.2kJ/mol, showing an upward trend with increased temperature.

When electrons continue to hit SF_5^-, R16 will occur: $SF_5^- + e \rightarrow SF_4^- + F^-$. When the temperature of R16 is 298K, △G is 32.2kJ/mol, when the temperature is increased

to 5000K, △G is −340.7kJ/mol, when the temperature reaches 10000K, △G is −589.2 kJ/mol. At 298K, the △G of this reaction is very low and it is likely to take place. With increase in temperature, the reaction can proceed spontaneously.

When the energy of electrons hitting SF_5 is high, $SF_5 + e \rightarrow SF_5^-$ reaction will occur first, and then SF_5^- will be decomposed as a result of the huge energy of electrons, and three reactions R13-R15 may occur: $SF_5^- \rightarrow SF_4^- + F$、$SF_5^- \rightarrow SF_4 + F^-$、$SF_5^- \rightarrow SF_4 + F + e$. When the temperature is 298K, the △G of R13 is 346.4kJ/mol, when the temperature rises to about 2600K, it drops to 0 kJ/mol, and when the temperature reaches 10000K, the △G is −1062.2 kJ/mol. The △G of R14 at 298K is 215.9 kJ/mol, when the temperature rises to about 2300K, it drops to 0 kJ/mol, and when the temperature reaches 10000K, the △G is −756 kJ/mol. The △G of R15 at 298K is 530.1 kJ/mol, when the temperature rises to about 3500K, it drops to 0 kJ/mol, and when the temperature reaches 10000K, the △G is −1229.1 kJ/mol. In the temperature range of 298–3250K, the △G of R14 is the lowest, so there is a high likelihood of occurrence. The reaction produces SF_4 and F^-. At 3250–6700K, the △G of R13 is the lowest, and the probability of occurrence of R13 is higher in this temperature range. When the temperature continues to rise to 6700–10000K, the probability of R15 is greatest.

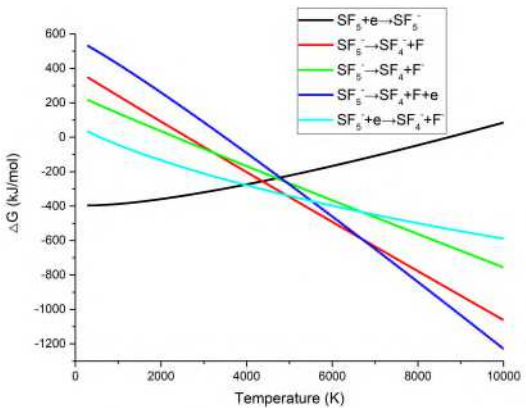

Figure 6. SF_5 electron impact decomposition process

△G changes with temperature

Figure 7 shows the change of ΔG of the R20-R24 reaction at a temperature of 298–10000K. It can be seen from Figure 7 that the △G of R21-R24 displays a downward trend with increasing temperature, but the △G of R20 rises with increasing temperature. When the electron energy in the space is low, the R20 reaction will occur: $SF_4 + e \rightarrow SF_4^-$. When the temperature is 298K, the △G is −183.7 kJ/mol, when the temperature is increased to 5000K, the △G is −73kJ/mol, when the temperature reaches 10000K, the △G is 166.8kJ/mol, showing an upward trend with increased temperature.

When electrons continue to hit SF_4^-, R24 will occur: $SF_4^- + e \rightarrow SF_3^- + F^-$. When the temperature of R24 is 298K, △G is −110.9kJ/mol, when the temperature is increased to 5000K, △G is −284.4kJ/mol, when the temperature reaches 10000K, △G is −319.3 kJ/mol. The △G of this reaction is less than zero, so it can carry on spontaneously.

When the energy of electrons hitting SF_4 is high, the $SF_4 + e \rightarrow SF_4^-$ reaction will take place first, and then SF_4^- will be decomposed due to the huge energy of the electrons, and three reactions R21-R23 may occur: $SF_4^- \rightarrow SF_3^- + F$, $SF_4^- \rightarrow SF_3 + F^-$, $SF_4^- \rightarrow SF_3 + F + e$. When the temperature of R21 is 298K, △G is 203.3kJ/mol, with a rise to about 2200K, it drops to 0 kJ/mol, when the temperature reaches 10000K, △G is −792.3 kJ/mol. The △G of R22 at 298K is 242.1 kJ/mol, when the temperature rises to about 2700K, it drops to 0 kJ/mol, and when the temperature reaches 10000K, the △G is −687.4 kJ/mol. The △G of R23 at 298K is 556.3 kJ/mol, with the temperature rise to about 3700K, it drops to 0 kJ/mol, and when the temperature reaches 10000K, the △G is −1160.4 kJ/mol. In the temperature range of 298–5800K, the ΔG of R21 is the lowest, so it

has the highest likelihood to take place. The reaction produces SF3- and F. The ΔG of R23 is the lowest at 5800–10000K, and the probability of occurrence of R23 is the highest in this temperature range.

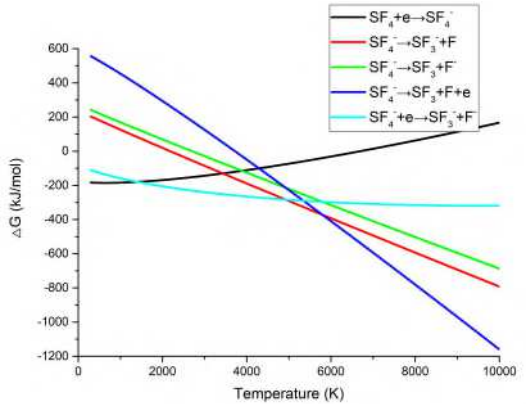

Figure 7. SF_4 electron impact decomposition process △G changes with temperature

Figure 8 shows the change of the ΔG of the R28-R32 reaction at a temperature of 298–10000K. It can be seen from Figure 8 that the △G of R29-R32 shows a downward trend with temperature rise, but the △G of R28 increases with increasing temperature. When the electron energy in the space is low, the R28 reaction will occur: $SF_3 + e \rightarrow SF_3^-$. When the temperature is 298K, △G is −353 kJ/mol, when the temperature rises to 5000K, △G is −63.6kJ/mol, when the temperature reaches 10000K, △G is 368.1kJ/mol, showing an upward trend as the temperature rises. When electrons continue to hit SF3-, R32 will occur: $SF_3^- + e \rightarrow SF_2^- + F^-$. When the temperature of R32 is 298K, △G is −111.9kJ/mol, on increasing it to 5000K, △G is −28.8kJ/mol, when the temperature reaches 10000K, △G is −4.5 kJ/mol. The △G of this reaction is less than zero, so it can proceed spontaneously.

When the energy of electrons hitting SF_3 is high, the $SF_3 + e \rightarrow SF_3^-$reaction will occur first, and then SF_3^- will decompose as a result of the huge energy of the electrons, and three reactions R29-R31 may occur: $SF_3^- \rightarrow SF_2^- + F$, $SF_3^- \rightarrow SF_2 + F^-$, $SF_3^- \rightarrow SF_2 + F + e$. The △G of R29 at 298K is 426.1kJ/mol, when the temperature rises to about 4600K, it drops to 0 kJ/mol, and with the temperatures at 10000K, the △G is −477.6 kJ/mol. The △G of R30 at 298K is 183.3kJ/mol, when the temperature rises to about 2000K, it drops to 0 kJ/mol, and when the temperature reaches 10000K, the △G is −791.4 kJ/mol. The △G of R31 at 298K is 497.5 kJ/mol, when the temperature rises to about 3300K, it drops to 0 kJ/mol, and when the temperature reaches 10000K, the △G is −1264.5 kJ/mol. In the temperature range of 298–5000K, R30 has the lowest △G, so it has the highest occurrence likelihood. The reaction produces SF_2 and F^-. The G of R31 is the lowest at 5000–10000K, and the probability of occurrence of R31 is the highest in this temperature range.

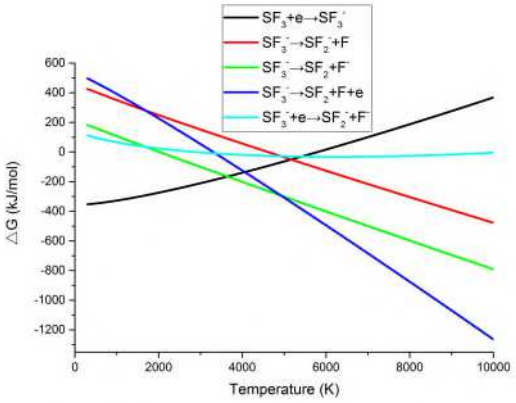

Figure 8. SF_3 electron impact decomposition process △G changes with temperature

Figure 9 shows the change of ΔG of the R36-R40 reaction at a temperature of 298–10000K. It can be seen from Figure 9 that the △G of R37-R40 shows a downward trend with increasing temperature, but the △G of R36 increases with increasing temperature. With a low electron energy in the space, the R36 reaction will occur: $SF_2 + e \rightarrow SF_2^-$. When the temperature is 298K, the △G is −71.4 kJ/mol, when the temperature is increased to 5000K, the △G is 272.6kJ/mol, when the temperature reaches 10000K, the △G is 786.9kJ/mol, showing an upward trend with

the increase of temperature.

When electrons continue to hit SF_2^-, R40 will occur: $SF_2^- + e \rightarrow SF^- + F^-$. When the temperature of R40 is 298K, △G is 64.3kJ/mol, when the temperature is increased to 5000K, △G is −191.6kJ/mol, and when the temperature reaches 10000K, △G is −363.6 kJ/mol. When the temperature is 298K, the ΔG of the reaction is high, when the temperature increases, the ΔG decreases, and the reaction can proceed spontaneously.

When the energy of electrons hitting SF_2 is high, the $SF_2 + e \rightarrow SF_2^-$ reaction will occur first, and then SF_2^- will be decomposed because of the huge electrons' energy, and three reactions R37-R39 may occur: $SF_2^- \rightarrow SF^- + F$, $SF_2^- \rightarrow SF + F^-$, $SF_2^- \rightarrow SF + F + e$. The △G of R37 at 298K is 170.3kJ/mol, when the temperature rises to about 1750K, it drops to 0 kJ/mol, and when the temperature reaches 10000K, the △G is −1072.8kJ/mol. The △G of R38 at 298K is 60.7kJ/mol, when the temperature rises to about 850K, it is reduced to 0 kJ/mol, and when the temperature reaches 10000K, the △G is −1098.5 kJ/mol. The △G of R39 at 298K is 374.9 kJ/mol, when the temperature rises to about 2500K, it reduces to 0 kJ/mol, and when the temperature reaches 10000K, the △G is −1571.6 kJ/mol. The temperature is in the range of 298–4900K, and R38 has the lowest △G, so it has the highest occurrence likelihood. The reaction produces SF and F-. The △G of R39 is the lowest at 4900–10000K, and the probability of occurrence of R39 is the highest in this temperature range.

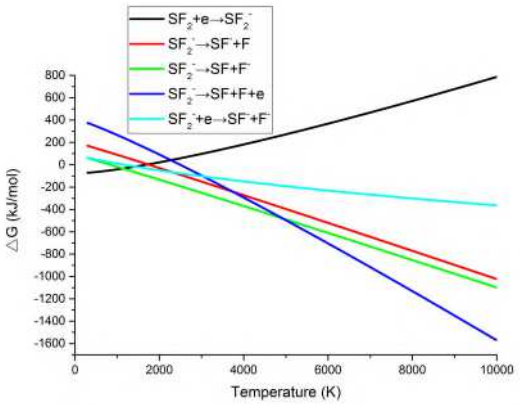

Figure 9. SF_2 electron impact decomposition process △G changes with temperature

Figure 10 shows the change of △G in the R44-R48 reaction at a temperature of 298–10000K. It can be seen from Figure 10 that the △G of R45-R48 shows a downward trend when the temperature is increased, but the △G of R44 increases with increasing temperature. When the electron energy in the space is low, the R44 reaction will occur: $SF + e \rightarrow SF^-$. When the temperature is 298K, △G is −204.6 kJ/mol, when the temperature rises to 5000K, △G is 100.2kJ/mol, when the temperature reaches 10000K, △G is 548.8kJ/mol, showing an upward trend with increasing temperature.

When electrons continue to hit SF-, R48 will occur: $SF^- + e \rightarrow S^- + F^-$. When the temperature of R48 is 298K, △G is 9.9kJ/mol, when the temperature is increased to 5000K, △G is −140.2kJ/mol, with the temperatures at 10000K, △G is −200.6kJ/mol. At 298K, the ΔG of the reaction is relatively low. As the temperature increases, the ΔG decreases to below 0, which was easy to occur.

When the energy of the electrons hitting the SF is high, the $SF + e \rightarrow SF^-$ reaction will occur first, and then the SF- will decompose because of the huge energy of the electrons, and three reactions R37-R39 may occur: $SF^- \rightarrow S^- + F$, $SF^- \rightarrow S + F^-$, $SF^- \rightarrow S + F + e$. The △G of R45 at 298K is 324.1kJ/mol, when the temperature rises to about 3600K, it is

minimized to 0 kJ/mol, and when the temperature reaches 10000K, the △G is −673.6kJ/mol. The △G of R46 at 298K is 193.2kJ/mol, when the temperature rises to about 2300K, it goes down to 0 kJ/mol, and when the temperature reaches 10000K, the △G is −781.3 kJ/mol. The △G of R47 at 298K is 507.4 kJ/mol, when the temperature rises to about 3500K, it drops to 0 kJ/mol, and when the temperature reaches 10000K, the △G is −1254.4 kJ/mol. In the temperature range of 298–4900K, R46 has the lowest ΔG, so it is most probable to take place. The reaction produces S and F-. The △G of R47 is the lowest at 4900–10000K, and the probability of occurrence of R47 is the highest in this temperature range.

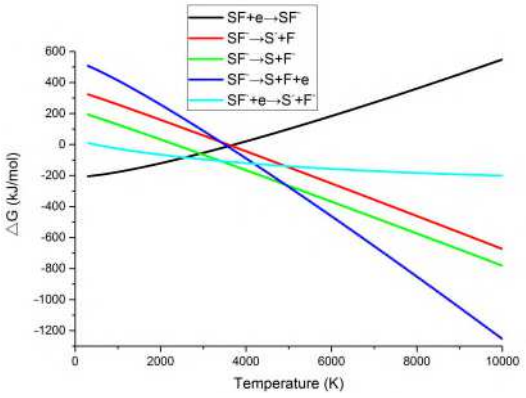

Figure 10. SF electron impact decomposition process △G changes with temperature

We have noticed, The △G of R4(SF_6 + e→SF_6^-) gradually decreases with the increase of temperature, but the △G of SF_n + e→SF_n^- (n＜6) increases with increasing temperature. The △G of a chemical reaction is defined as

$$\Delta G = \Delta H - \Delta TS$$

Among them, △H is the enthalpy change, T is the temperature, and △S is the entropy change. Through the previous calculations, we obtained the △H and △S of all reaction processes at the same time, and the entropy of electrons was obtained in Fifen's article. Figure 11-13 is obtained by calculating other thermodynamic data of these six reactions. From Figure 11, it can be found that the ΔH of these six reactions decreases with the increase of temperature, and the rate of decrease is almost the same, and they are all less than zero. From Figure 12, it can be found that the entropy changes of these six reactions all decrease with the increase of temperature. The difference is that the entropy change of R4 is always greater than 0 in the temperature range of 298-10000K, while the entropy change of SF_n + e→SF_n^- (n＜6) is less than 0 with increasing temperature. It can also be seen from Figure 13 that the rate of decrease of △T·S product of R4 is much lower than that of the other five reactions, and the decrease rate of the △T·S is lower than that of ΔH. It can be seen from the definition of free energy that the △G of R4 increases with increasing temperature. In the other five reactions, the △T·S decrease rate is greater than the decrease rate of ΔH, that is, the increase rate of −△T·S is greater than the decrease rate of ΔH. Therefore, the △G of SF_n + e→SF_n^-(n＜6) increases with increasing temperature.

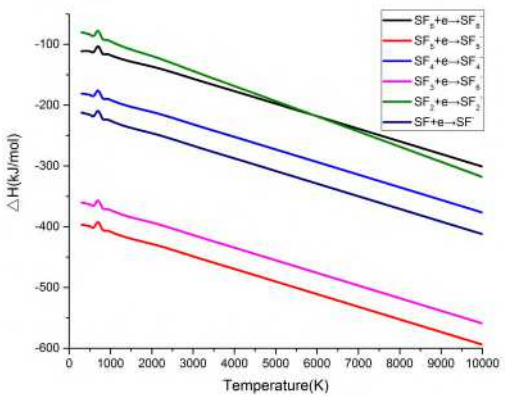

Figure 11. △H of SF_n + e→SF_n^- varies with temperature

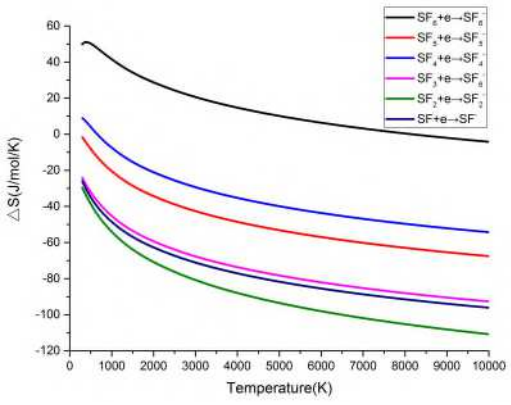

Figure 12. △S of $SF_n + e \rightarrow SF_n^-$ varies with temperature

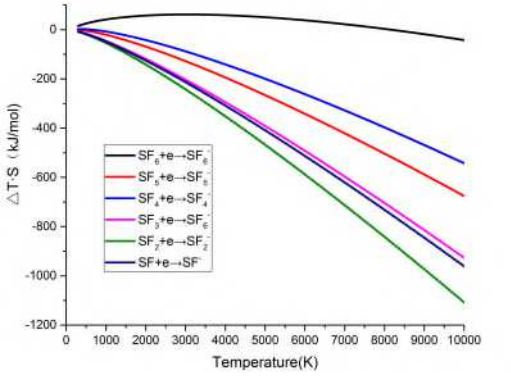

Figure 13. △T·S of $SF_n + e \rightarrow SF_n^-$ varies with temperature

4. CONCLUSION

This paper uses quantum chemistry theory to study the reaction mechanism of SF_n thermal decomposition and electrical decomposition at 298–10000 K, including a total of 17 particles and 48 chemical reactions. The Gibbs free energy data of electrons are acquired by cubic spline difference fitting, and the electrons are taken into account in the reaction equation. Structural optimizations, vibrational frequency calculations, and zero-point energy calculations for the reactants and products were performed at the B3LYP/6-311++G(d,p) level of theory. The single-point energies of all species were obtained at the CCSD(T)/aug-cc-PVTZ level. The frequency vibration factor (0.967) is taken into consideration. The main conclusions drawn are:

(1) In the temperature range of 298–10000K, the △G of SF_n thermal decomposition and homocracking reaction starts to decrease from 200kJ/mol, while the △G of the other two heterocracking reactions starts to decrease from 1000kJ/mol and 2000kJ/mol respectively. Both show a downward trend with an almost similar slope, and homolytic reaction is more likely to occur.

(2) In the temperature range of 298–10000K, the SF_n electron impact decomposition process can be divided into three possibilities based on the size of the electron energy. When the electron energy is low, $SF_n + e \rightarrow SF_n^-$ occurs, and the △G of SF_5, SF_4, SF_3, SF_2, SF decomposition reaction increases with the rise in temperature, while the △G of SF_6 decomposition decreases with increasing temperature.

(3) When the electron energy is high, the electrons hitting SF_n will not generate SF_n^- but directly decompose SF_n^- :
In the temperature range of 298–8700k, △G of R5 is lowest, so it has the highest probable occurrence. SF_6^- decomposition produces SF_5^- and F. In the temperature range of 8700–10000K, △G of R7 is the lowest, and R7 has a greater probability of occurrence in this temperature range.

(4) In the temperature range of 298–3250K, the △G of R14 is the lowest, so it will most likely occur. SF_5^- decomposes to produce SF4 and F^-. In the temperature range of 3250–6700K, the △G of R13 is the lowest, and the probability of occurrence of R13 is greater in this temperature range. SF_5^-decomposes to produce SF_4^- and F. When the temperature continues to rise to 6700–10000K, the probability of occurrence of R15 is greatest.

(5) In the temperature range of 298–5800K, the ΔG of R21 is the lowest, so it has the highest occurrence likelihood. SF_4^- decomposes to produce SF3- and F. In the temperature range of 5800–10000K, the △G of R23 is the lowest, and the probability of occurrence of R23 is the highest in this temperature range.

(6) In the temperature range of 298–5000K, R30 has the lowest △G, so it is most probable to occur. SF_3^- decomposition produces SF_2 and F^-. In the temperature range of 5000–10000K, the △G of R31 is the lowest, and the probability of occurrence of R31 is the highest in this temperature range.

(7) In the temperature range of 298–4900K, R38 has the lowest △G, so it is most likely to occur. SF_2^- generates SF and F^-. In the temperature range of 4900–10000K, the △G of R39 is the lowest, and the probability of occurrence of R39 is the highest in this temperature range.

(8) In the temperature range of 298–4900K, R46 has the lowest ΔG, thus it has the highest occurrence likelihood. The decomposition of SF^- produces S and F^-. In the temperature range of 4900–10000K, the △G of R47 is the lowest, and the probability of occurrence of R47 is the highest in this temperature range.

(9) When the second electron hits SF_n^-, the $SF_n^- + e \rightarrow SF_{n-1}^- + F^-$ occurs. And the ΔG of the reaction gradually decreases with the increase of temperature. The ΔG of this series of reactions is lower and more likely to occur.

This work provides a reference for studying the by-products of the reaction of SF_6 with micro water or micro oxygen.

SUPPLEMENTARY MATERIAL

See the supplementary material for the thermal decomposition reaction of SF_4, SF_3, SF_2, and SF in detail.

Declarations

Funding

The authors declare that this study was not funded.

Conflicts of interest/Competing interests

The authors declare that they have no known competing financial interests or personal relationships that could have appeared to influence the work reported in this paper.

Availability of data and material

The data that support the findings of this study are available within the article.

Code availability

The author's organization owns the copyright of the software program used in the article, and there is no custom code in this article.

Authors' contributions

There were equal contributions of the authors to the completion of this work.

REFERENCES

1. H. D. Lin Tao, Zhong Haifeng, Qi Yao, and Zhang Guoqiang, Transactions of China Electrotechnical Society **29** (2), 219-225 (2014).

2. T. Ziegler and G. L. Gutsev, The Journal of Chemical Physics **96** (10), 7623-7632 (1992).

3. L. N. M. Piemontesi, in *1996 IEEE International Symposium on Electrical Insulation* (IEEE, MONTREAL, CANADA, 1996), pp. 828-838.

4. Y. Qiu and E. Kuffel, IEEE Transactions on Dielectrics and Electrical Insulation **6** (6), 892-895 (1999).

5. B. Belmadani, J. Casanovas and A. M. Casanovas, IEEE Transactions on Electrical Insulation **26** (6), 1177-1182 (1991).

6. R. L. Wilkins, The Journal of Chemical Physics **51** (2), 853-854 (1969).

7. W. Frie, Zeitschrift fr Physik **201** (3), 269-294 (1967).
8. A. J. Ahearn and N. B. Hannay, The Journal of Chemical Physics **21** (1), 119-124 (1953).
9. N. Wiegart, L. Niemeyer, F. Pinnekamp, J. Kindersberger, R. Morrow, W. Zaengl, M. Zwicky, I. Gallimberti and S. A. Boggs, IEEE Transactions on Power Delivery **3** (3), 923-930 (1988).
10. Y. Wang, R. L. Champion, L. D. Doverspike, J. K. Olthoff and R. J. Van Brunt, The Journal of Chemical Physics **91** (4), 2254-2260 (1989).
11. J. J. Fifen, J Chem Theory Comput **9** (7), 3165-3169 (2013).
12. X. Wang, Q. Gao, Y. Fu, A. Yang, M. Rong, Y. Wu, C. Niu and A. B. Murphy, Journal of Physics D: Applied Physics **49** (10) (2016).
13. A. D. Becke, Phys Rev A Gen Phys **38** (6), 3098-3100 (1988).
14. F. C. Pickard, D. R. Griffith, S. J. Ferrara, M. D. Liptak, K. N. Kirschner and G. C. Shields, International Journal of Quantum Chemistry **106** (15), 3122-3128 (2006).
15. S. Canneaux, F. Bohr and E. Henon, J Comput Chem **35** (1), 82-93 (2014).
16. Y. S. Cheung, Y. J. Chen, C. Y. Ng, S.-W. Chiu and W.-K. Li, Journal of the American Chemical Society **117** (38), 9725-9733 (1995).
17. M. J. Frisch, G. W. Trucks, et al. Gaussian 09, Revision A.02, Gaussian, Inc. Wallingford CT, 2009.
18. National Insitute of Standards and Technology 2018 NIST chemistry webbook. https://webbook.nist.gov/chemistry
19. S. Y. Ye, F. Z. Deng, Journal of Huaibei Coal Teachers College (Natural Science Edition),(01):71-74, 1992.

Figures

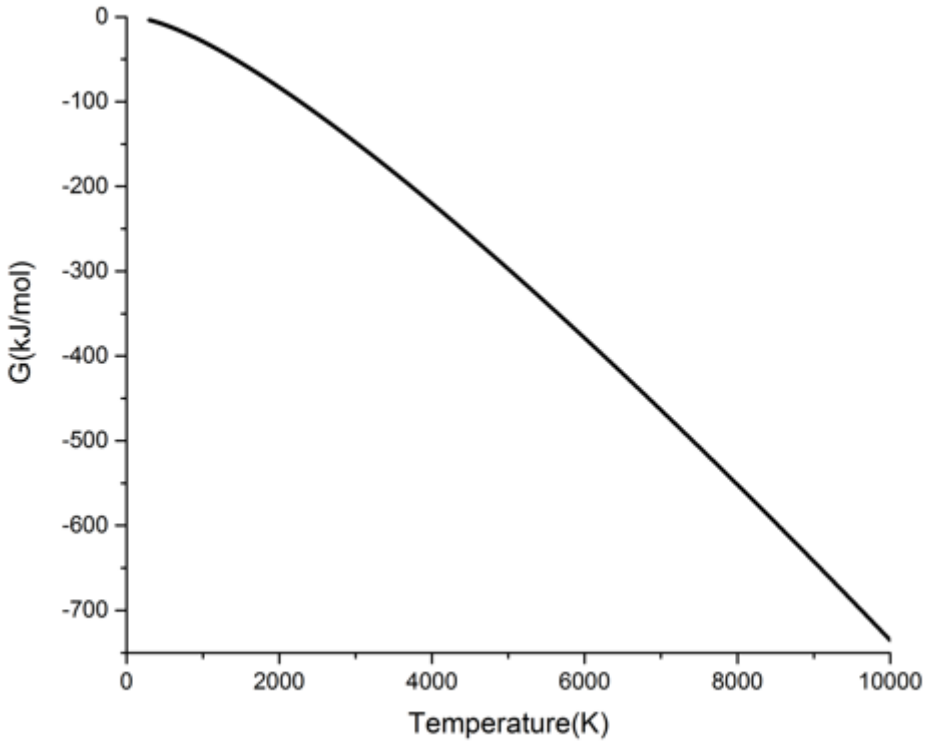

Figure 1

Gibbs free energy of gas phase electrons changes with temperature

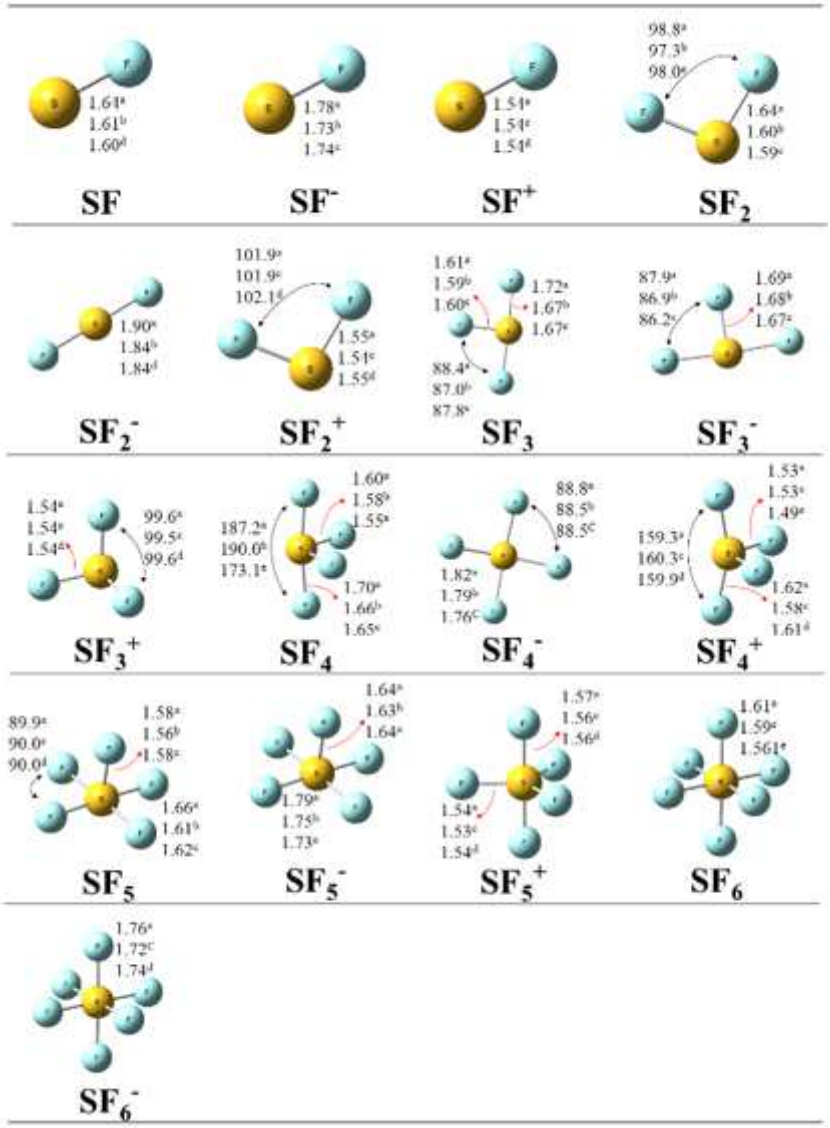

Figure 2

Optimized structures of all reactants and products. (Bond lengths are in angstroms and bond angles are in degrees.)

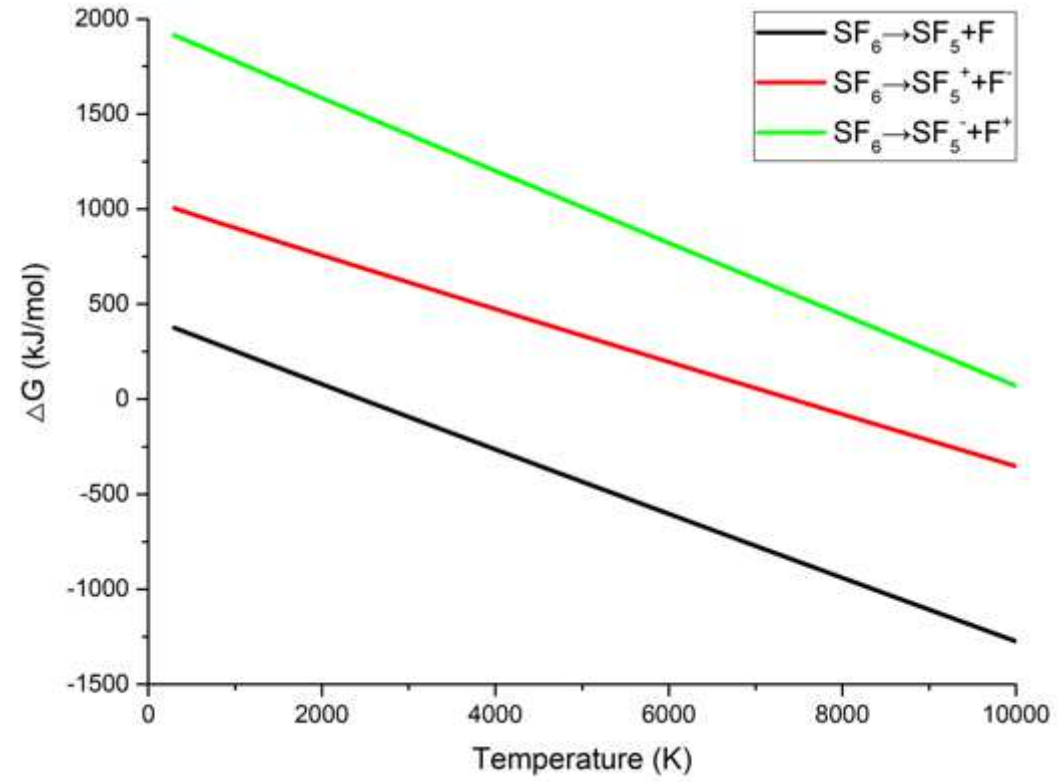

Figure 3

SF6 thermal decomposition △G changes with temperature

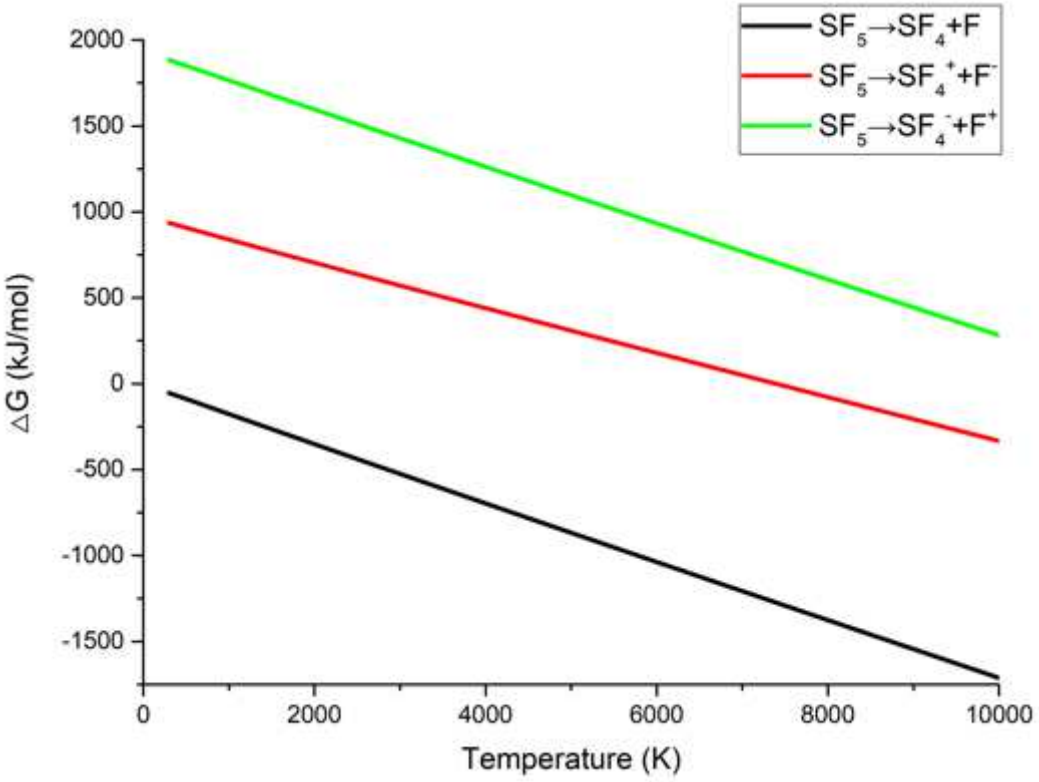

Figure 4

SF5 thermal decomposition △G changes with temperature

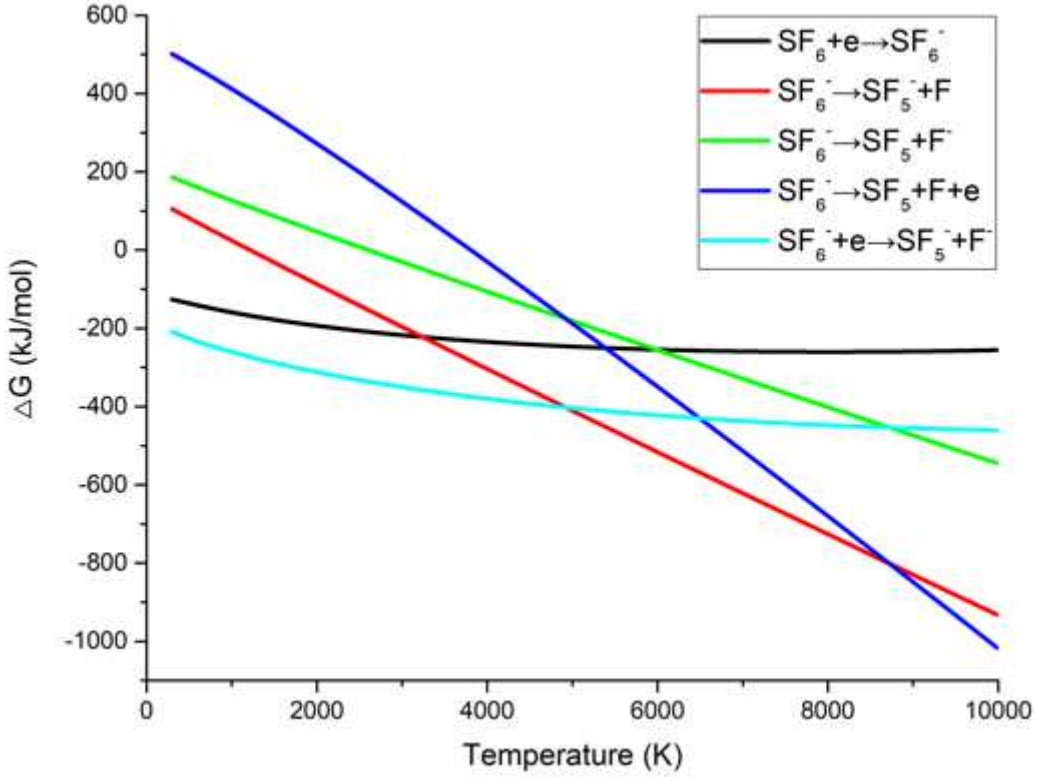

Figure 5

SF6 electron impact decomposition process △G changes with temperature

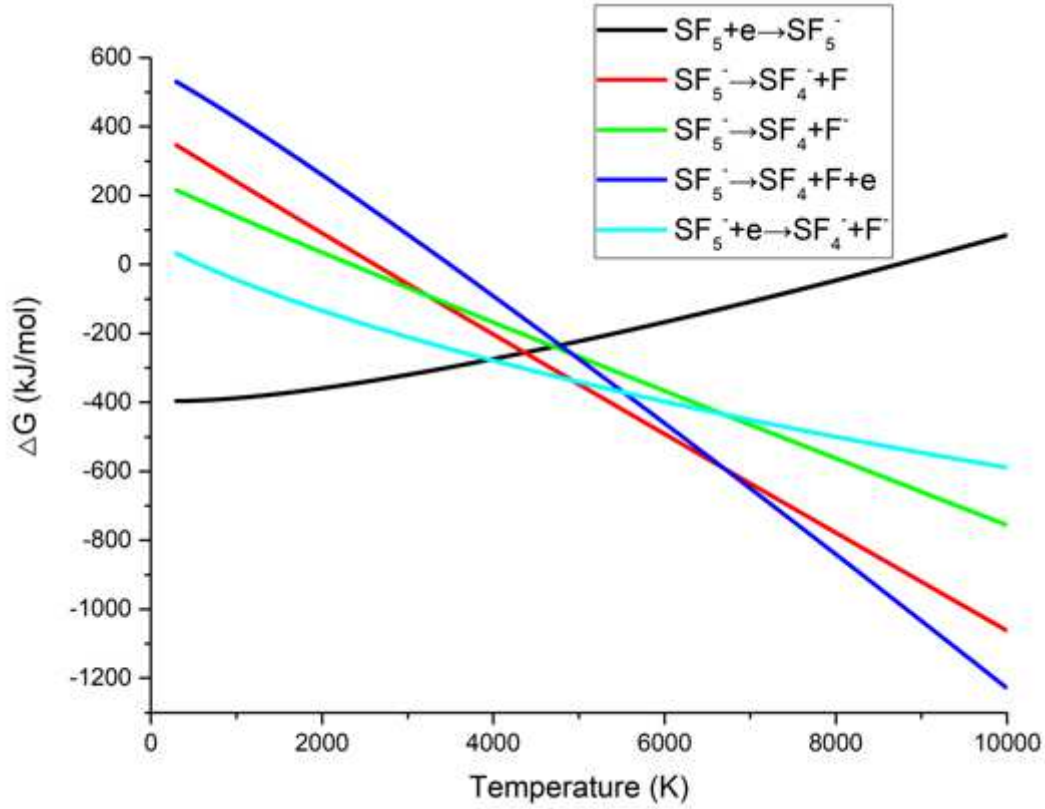

Figure 6

SF5 electron impact decomposition process

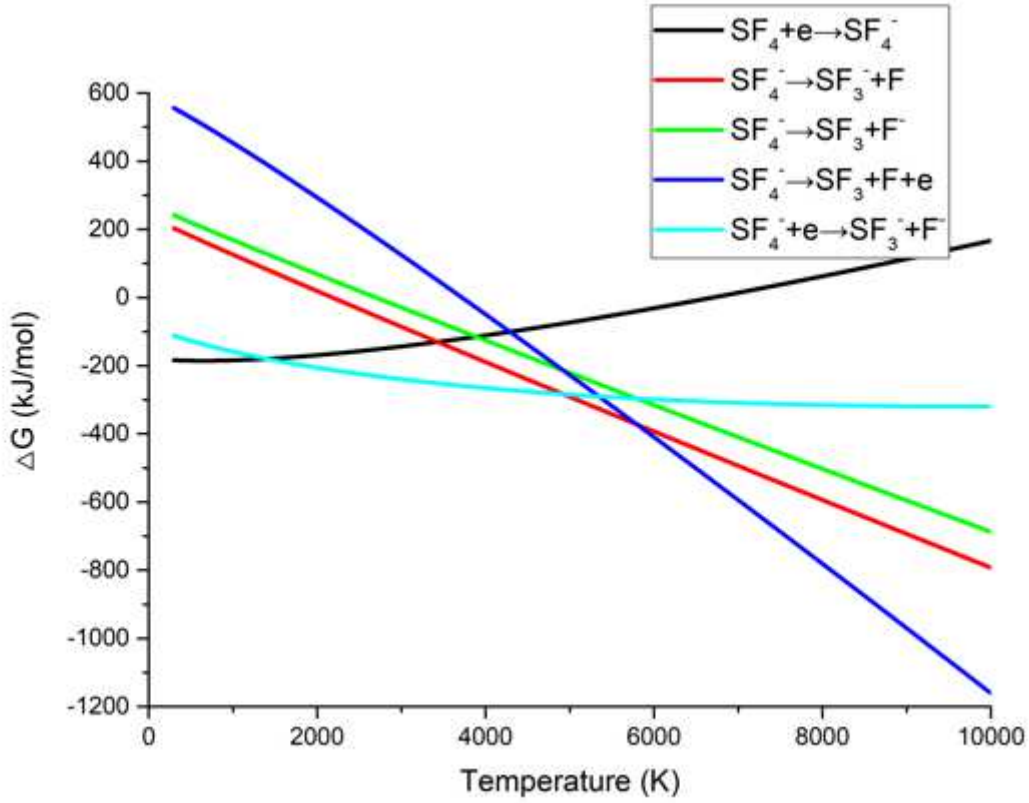

Figure 7

SF4 electron impact decomposition process △G changes with temperature

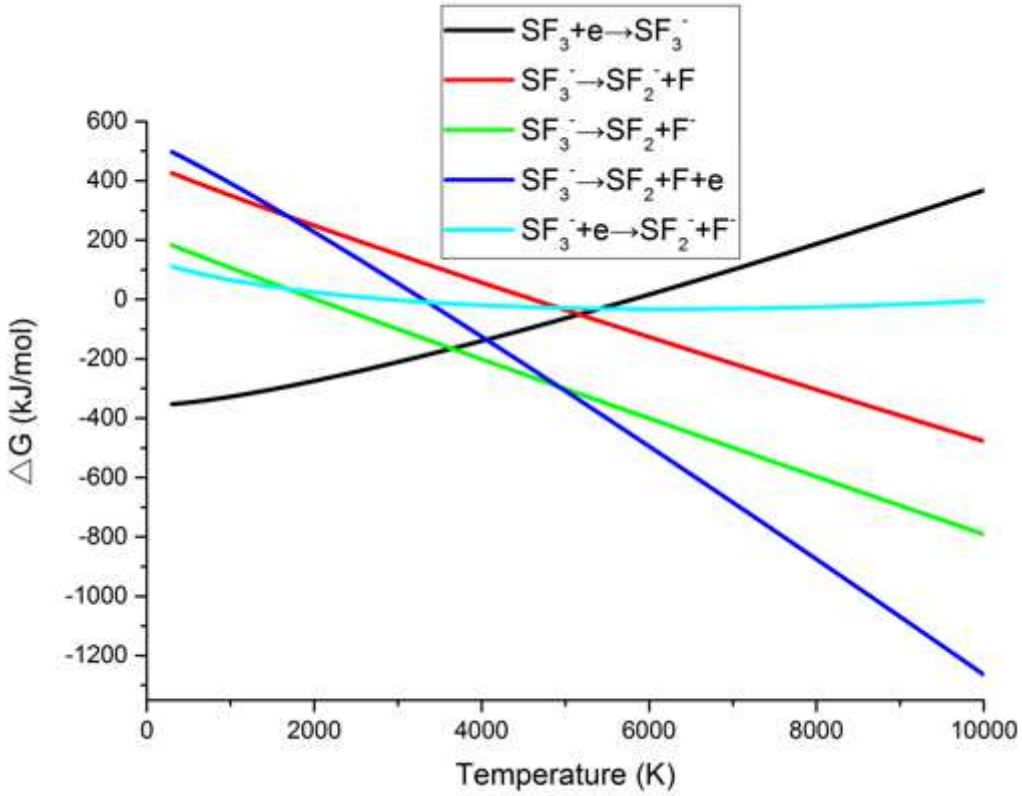

Figure 8

SF3 electron impact decomposition process △G changes with temperature

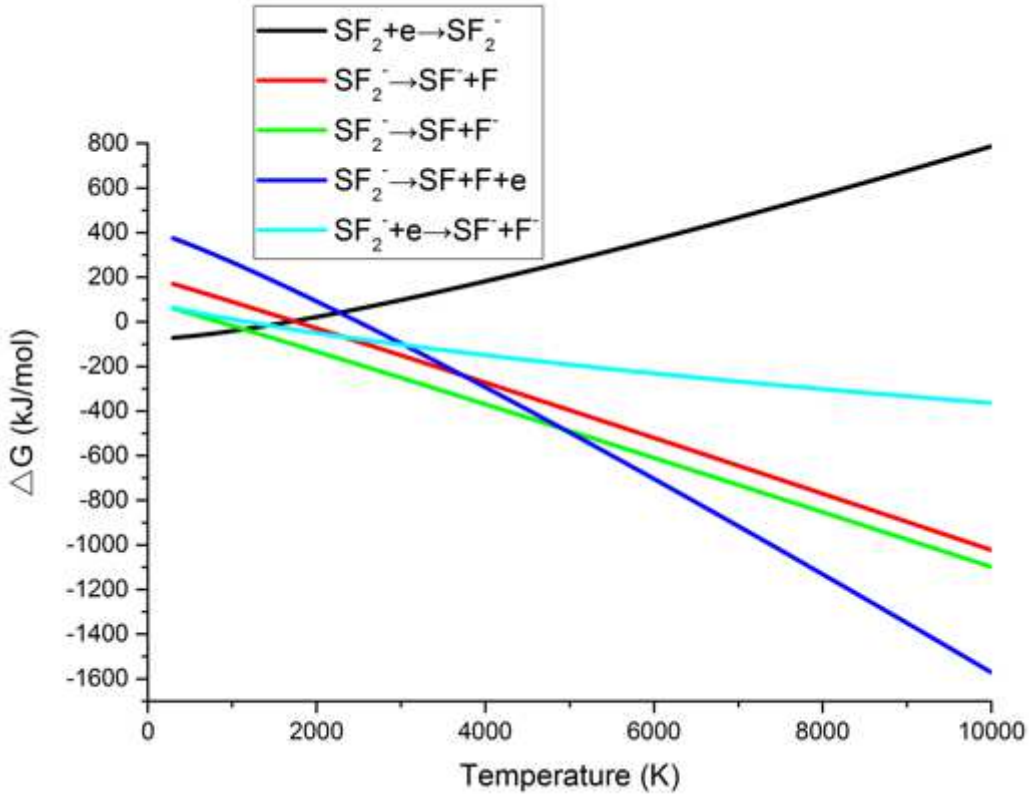

Figure 9

SF2 electron impact decomposition process ΔG changes with temperature

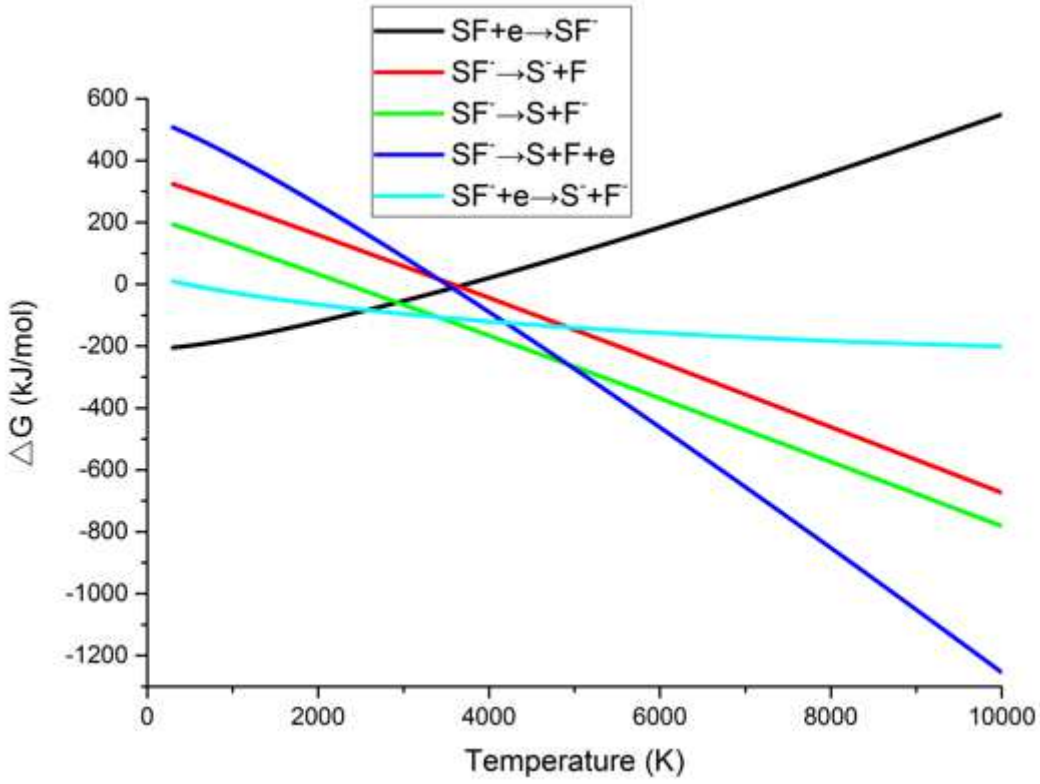

Figure 10

SF electron impact decomposition process ΔG changes with temperature

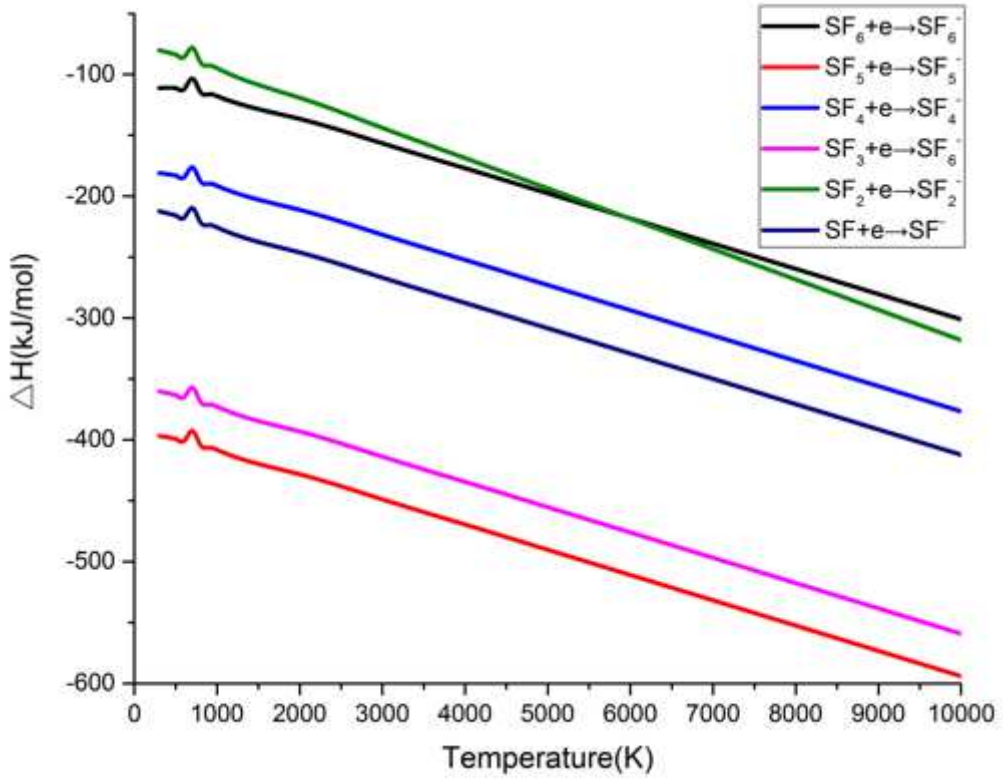

Figure 11

H of SFn + e SFn- varies with temperature

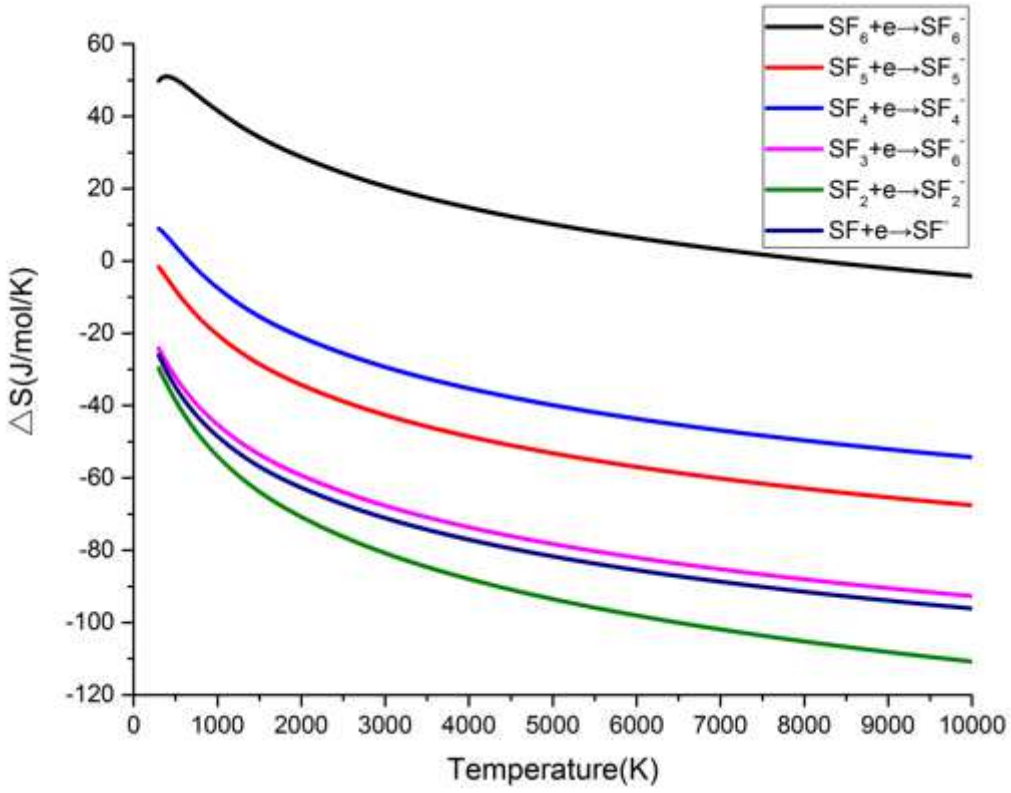

Figure 12

S of SFn + eSFn- varies with temperature

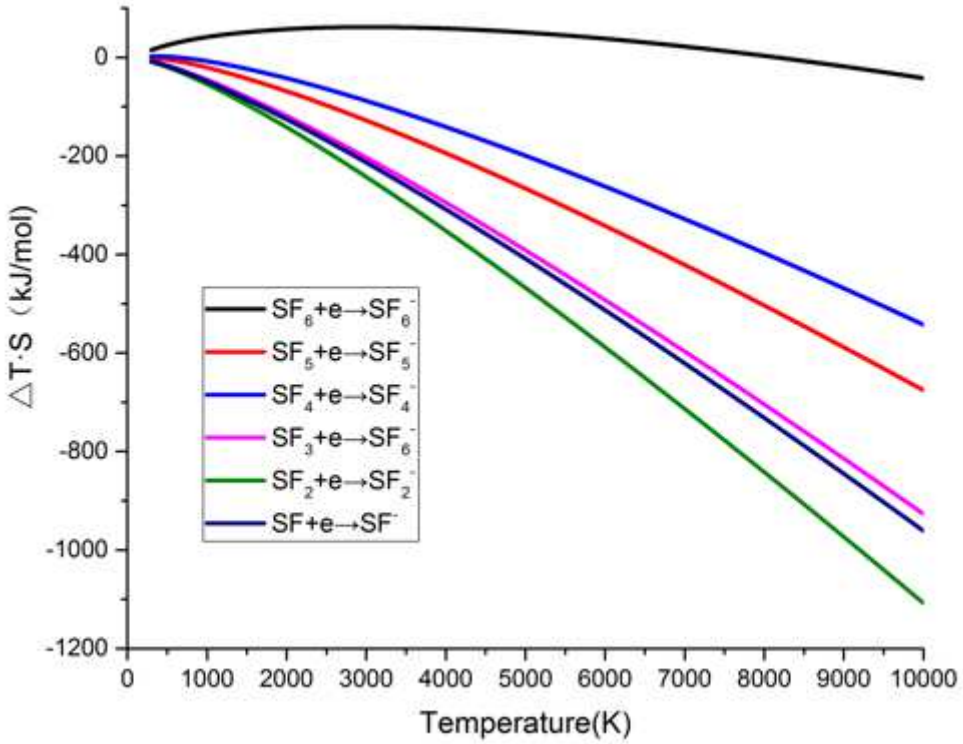

Figure 13

T·S of SFn + eSFn- varies with temperature

Supplementary Files

This is a list of supplementary files associated with this preprint. Click to download.

- Supplementarymaterials.docx